Immunology and Inflammation
Computational and Systems Biology

Thrifty wide-context models of B cell receptor somatic hypermutation

Reviewed Preprint
v1 • March 18, 2025
Not revised

Kevin Sung, Mackenzie M Johnson, Will Dumm, Noah Simon, Hugh Haddox, Julia Fukuyama, Frederick A Matsen IV

Computational Biology Program, Fred Hutchinson Cancer Center, Seattle, United States • Department of Biostatistics, University of Washington, Seattle, United States • Department of Statistics, Indiana University, Bloomington, United States • Howard Hughes Medical Institute, Seattle, United States • Department of Genome Sciences, University of Washington, Seattle, United States • Department of Statistics, University of Washington, Seattle, United States

eLife Assessment

This study provides an **important** method to model the statistical biases of hypermutations during the affinity maturation of antibodies. The authors show **convincingly** that their model outperforms previous methods with fewer parameters; this is made possible by the use of machine learning to expand the context dependence of the mutation bias. They also show that models learned from nonsynonymous mutations and from out-of-frame sequences are different, prompting new questions about germinal center function. Strengths of the study include an open-access tool for using the model, a careful curation of existing datasets, and a rigorous benchmark; it is also shown that current machine-learning methods are currently limited by the availability of data, which explains the only modest gain in model performance afforded by modern machine learning.

https://doi.org/10.7554/eLife.105471.1.sa3

Abstract

Somatic hypermutation (SHM) is the diversity-generating process in antibody affinity maturation. Probabilistic models of SHM are needed for analyzing rare mutations, for understanding the selective forces guiding affinity maturation, and for understanding the underlying biochemical process. High throughput data offers the potential to develop and fit models of SHM on relevant data sets. In this paper we model SHM using modern frameworks. We are motivated by recent work suggesting the importance of a wider context for SHM, however, assigning an independent rate to each k-mer leads to an exponential proliferation of parameters. Thus, using convolutions on 3-mer embeddings, we develop “thrifty” models of SHM that have fewer free parameters than a 5-mer model and yet have a significantly wider context. These offer a slight performance improvement over a 5-mer model. We also find that a per-site effect is not necessary to explain SHM patterns given nucleotide context. Also, the two current methods for fitting an SHM model — on out-of-frame sequence data and

on synonymous mutations — produce significantly different results, and augmenting out-of-frame data with synonymous mutations does not aid out-of-sample performance.

Introduction

Antibodies are an essential component of the adaptive immune response. They are secreted by B cells, and when displayed on the surface of B cells are called B cell receptors. When stimulated by antigen binding, B cells undergo a process called "affinity maturation" which involves mutation and selection. The mutation process happens at a very high rate relative to the rate of normal somatic mutation and is called somatic hypermutation (SHM). As such, it is an essential part of the adaptive immune response. It is generated by a complex collection of interacting pathways of DNA damage and error-prone repair, which have been elucidated through decades of research (Wagner and Neuberger, 1996; Teng and Papavasiliou, 2007; Methot and Di Noia, 2017; Pilzecker and Jacobs, 2019). These pathways lead to a very non-uniform distribution of mutations.

Furthermore, the mutation biases are predictable from local sequence context. Many papers have investigated predictors of mutation rates from molecular sequence, including early work establishing the biases (Dunn-Walters et al., 1998; Rogozin and Kolchanov, 1992; Rogozin and Diaz, 2004), to parametric models estimating the mutability based on local sequence "motif", or sequence neighborhood around a focal base (Yaari et al., 2013; Elhanati et al., 2015; Cui et al., 2016; Feng et al., 2019; Fisher et al., 2024).

Such models are important when predicting the probability of amino acid changes in affinity maturation, e.g. for understanding the prospects of selecting such mutations in for reverse vaccinology (Wiehe et al., 2018; Martin Beem et al., 2023) or in computing a model of natural selection on antibodies (McCoy et al., 2015; Hoehn et al., 2017, 2019).

The most popular models for somatic hypermutation are the S5F 5-mer model and its variants (Yaari et al., 2013; Cui et al., 2016). They have shown their worth for over a decade now, including tasks such as predicting the probability of mutations to mature broadly neutralizing antibodies against HIV (Wiehe et al., 2018, 2022). However, biological considerations suggest that a wider context should be considered.

Indeed, the consensus view of SHM requires processes such as patch removal around an AID-induced lesion (Pilzecker and Jacobs, 2019) and error-prone repair. Thus, for example, the presence of an AID hotspot several bases away may influence the probability of a mutation at a focal base. More recently, mesoscale-level sequence effects on AID deamination potentially deriving from local DNA sequence flexibility have been discovered (Wang et al., 2023). In addition, other work has found that position in the sequence can influence SHM (Cohen et al., 2011; Zhou and Kleinstein, 2020; Spisak et al., 2020).

This begs the question of how one could use more complex models to predict somatic hypermutation. 7-mer models, which have 3 flanking bases on either side of the focal base, have been used (Elhanati et al., 2015; Marcou et al., 2018). However, one cannot simply increase the size of the k-mer model indefinitely because the number of parameters grows exponentially with the size of the k-mer. More recent models of somatic hypermutation include position-specific terms (Spisak et al., 2020) and context models of size up to 21 parameterized by a convolutional neural network (Tang et al., 2022). In other contexts, models based on the transformer architecture (Vaswani et al., 2017) have shown great success, raising the question of if such an architecture could be used here.

In this paper we develop new models using modern frameworks, and provide a comprehensive evaluation of the models. We especially focus on the development of parameter-efficient convolutional neural networks, which we call "thrifty" models. These models have wide nucleotide context yet can have fewer parameters than a 5-mer model, while providing slightly better performance on metrics in train and test time. On the other hand, we find that elaborations such as a per-site rate and transformer only harm out-of-sample performance. We also find a clear difference between training models to predict well on out-of-frame data, compared to training models to predict well on synonymous mutations. To make these models useful for the community, we have released an open-source Python package *https://github.com/matsengrp/netam* with pretrained models and a simple API. Our analysis for this paper is reproducible via *https://github.com/matsengrp/netam-experiments-1*.

Results

Overview of data preparation and objective

We will begin with an overview of our models and data. Full details are provided in the Methods.

Our objective in this project is to predict the probability of observed somatic hypermutation in a child sequence relative to a parent sequence. We follow previous work (Spisak et al., 2020) in overall goal and data setup. Specifically, we predict mutations in BCR sequences that are out-of-frame, i.e. such that the sequence cannot code for a productive receptor. Because the data is out-of-frame, this means that the sequences under consideration are less likely to have undergone selective pressure in the germinal centers, and instead provides more information about the SHM process. We also provide more relevant parent sequences and predict finer-scale events by using phylogenetic reconstruction and ancestral sequence inference on sequences clustered into clonal families (**Figure 1a**). We split the tree with ancestral sequences into pairs of parent and child sequences, which we call parent-child pairs. We also experiment with using synonymous mutation data by masking mutations from the loss function that are not synonymous (below; details in Methods).

In all models, the distribution of mutations at a particular site is assumed to be independent of mutations at all other sites (but not independent of context). We follow many authors starting from (Yaari et al., 2013) in estimating a per-site rate, as well as a per-site probability distribution among the non-identical bases describing the base selected in the event of a mutation. We will call this the conditional substitution probability (CSP). For each site i, we assume that the mutation process is an Exponential waiting time process with rate λ_i. Once the mutation occurs, we assume that the base is selected according to a categorical distribution with probabilities $\mathbf{p}_i$. Similar assumptions have been made previously (Rosset, 2007; Levinstein Hallak et al., 2018; Spisak et al., 2020; Levinstein Hallak and Rosset, 2022). To accommodate evolutionary time in our model, we include *offsets* in our exponential model—if t is a branch length parameter for a sequence pair we use parameter $\tilde{\lambda} = t\lambda$ for model inference so that the model is able to learn λ irrespective of evolutionary time on a particular branch. This parameter t is frequently the normalized mutation count (as in Spisak et al., 2020) but can be optimized as part of a joint optimization.

We used two data sets, that we will call the briney and tang data sets. The briney data (Briney et al., 2019) consists of samples from 9 individuals, but 2 of these samples resulted in many more sequences than the rest. We will thus use a test-train split in which these 2 samples form the training data and the other 7 form the testing data. We acknowledge the important work the Spisak et al., 2020 team did in processing the briney data. The tang data (Vergani et al., 2017; Tang et al., 2020) will be a further test set. Details on data processing appear in the Methods. In the Methods, we describe our attempts to find additional data sets.

Models

We use the following strategy to combine the predictive power of local-context models without having the parameter penalty (**Figure 1b**). Each 3-mer is mapped into a embedding space of a fixed dimension, and these embedding locations are trainable parameters of the model. The idea is that the embedding abstracts some SHM-relevant characteristics of that 3-mer. Each sequence is then represented as a matrix with (sequence length) rows and (embedding dimension) columns. We then apply convolutional filters to these matrices, with taller convolutional filters effectively increasing the context of the model. For example, a kernel size of 11 gives effectively a 13-mer model (because of the additional base on either side of the 3-mer). We then apply a simple linear layer to the result of this step in order to get a mutation rate estimate for each site.

As described above, this class of models predicts both the per-site rate of SHM as well as the probability of alternate bases after mutation (called the CSP as above). We make these two model outputs in three ways (**Figure 1—figure Supplement 1**): they can share everything except for the final layer ("joined" model), or they can share the embedding layer ("hybrid" model), or they can be estimated separately ("independent" model). A key difference with a full k-mer model is that when we increase the size of the kernel, the number of parameters increases linearly, not exponentially. In this way, the thriftiest well-performing model is effectively a 13-mer model with fewer parameters than a 5-mer model, however one can scale these models among a variety of dimensions (**Table 1**).

We implemented our models in PyTorch (Paszke et al., 2019). Because of the small size of these models, they are fast to train and use.

Thrifty CNNs give a modest performance improvement

In order to evaluate our proposed methods and compare to previous work, we first characterized the models in terms of predictive performance using AUROC, AUPRC, R-precision, and substitution accuracy. AUROC, the area under the ROC curve, can be interpreted as the probability that the model correctly identifies sites that mutate as having higher mutability than those that do not. In fact, if one randomly selects a positive-negative pair, the AUROC is the probability that the positive example is assigned a higher probability than the negative example. However, this measure is sensitive to class imbalance, and we are in the imbalanced setting here because mutations are relatively rare. AUPRC, the area under the precision-recall curve, provides an alternative that is less sensitive to class imbalance effects (Saito and Rehmsmeier, 2015; Ozenne et al., 2015) because the precision is the fraction of positive predictions that are true positives. R-precision gives a sense of how accurate the model is among sites that are most mutable. Specifically, if a given PCP had R mutations, R-precision is the precision of the predictions of mutability at the R sites that are ranked as being most mutable. To evaluate performance at predicting per-base substitution probabilities (given a mutation occurred), we report substitution accuracy: how frequently is the predicted-most-likely base the one to which a site mutates?

We found that the thrifty CNN models gave a modest performance improvement for these predictive metrics compared to existing models (**Figure 2**, **Figure 2—figure Supplement 1**). Specifically, we compared to a 5-mer model trained in exactly the same way, as well as a reimplementation of the model of Spisak et al., 2020). We confirmed that our reimplementation infers very similar parameters to the previous implementation, although we add a slight regularization to avoid some aspects of the original model fit that appear to be artifacts (**Figure 2—figure Supplement 2**). Because the Spisak et al., 2020 model fits a per-site rate, and the briney data does not have full sequence coverage, we limited all evaluation to a region well covered by the briney data: positions 80 to 319, inclusive.

release name: paper name	Kernel	Embed	Filters	Dropout	Params
ThriftyHumV0.2-20: CNN Joined Large	11	7	19	0.3	2,057
5mer	-	-	-	-	3,077
Spisak	-	-	-	-	3,576
ThriftyHumV0.2-45: CNN Indep Medium	9	7	16	0.2	4,539
ThriftyHumV0.2-59: CNN Indep Large	11	7	19	0.3	5,931

Table 1.

Selected model shapes and dropout probabilities.

The release name of the model is the name of the trained model released in the GitHub repository; upon publication of this paper we will release V1.0. The paper name is the name of the model used in this manuscript, which describes more about its architecture. “Kernel”: the size of the convolutional kernel used in the model. “Embed”: the size of the embedding used for each 3-mer. Because there is one additional base on either side of a 3-mer, a model with kernel size 9 is effectively an 11-mer model, and a model with kernel size 11 is effectively a 13-mer model.

We were surprised to find that all metrics except substitution accuracy were better on data from a distinct sequencing experiment (tang data) than on held-out samples from the same sequencing experiment (briney data). We attribute this to there being a difference in sequencing error between the two experiments. The briney data allowed sequences with only a single UMI representative (Spisak et al., 2020) while the tang data required at least two sequences per UMI (Tang et al., 2020). If our model is successfully learning substitution probabilities due to SHM rather than the sequencing error, we would expect our model to under-estimate the number of substitutions at positions with a low probability of substitution in the briney data (which we expect to have more sequencing error) but not in the tang data (which we expect to have less sequencing error). This is in fact what we see in our characterization of model fit below. We were also surprised to find that the per-site rate did not seem to help the 5-mer model on held-out data, despite the results of Spisak et al., 2020; see Discussion.

We did not see a substantial performance improvement by increasing the number of parameters of the CNNs. Recall that our models differ in terms of how much they share between predicting the position of mutations and predicting their base identity (**Figure 1—figure Supplement 1**). Although the "Large Indep" model that has the most flexibility may do a slightly better job with held-out samples from the same experiment in terms of substitution accuracy, it doesn't appear any better when considering data from another experiment.

We also compared our work to a previous deep neural network model of SHM (Tang et al., 2022), which was trained on the tang data set. A DeepSHM model consists of a pair of CNN models, one for estimating mutation frequencies and another for CSPs; this is akin to our "independent" model configuration. Each of these CNNs has over 250,000 parameters, so in total is about 100 times larger than the largest CNN model we trained. These CNNs are also slow to evaluate: because they make predictions one k-mer at a time, one must iterate over the sequence and obtain predictions for every site. Because the DeepSHM model cannot handle ambiguous nucleotides, we had to remove these from the evaluation. The authors found the best performance is achieved with 15-mers, which is comparable with the 11-mers and 13-mers in our thrifty models. We evaluated the DeepSHM 15-mer model on the subset of the briney data and found it performs better than S5F but comparable to our models (**Table 2**). Specifically, our models performed comparably when trained on the tang data only, but when trained on the combined tang data and briney two largest repertoires, our models performed slightly better on the briney held-out repertoires.

We next characterized models in terms of out-of-sample model fit. For each site in the parent of each parent-child pair (PCP) of sequences, we computed the probability of a nucleotide substitution at that site in the corresponding child. We then compared the sum of those probabilities to the actual number of substitutions that were observed at each site in the PCPs (**Figure 3**). If the observed and expected counts match, then the model is doing a good job, on average, of predicting site-specific probabilities of substitution. We assessed matching using an "overlap" metric, which quantifies the size of the intersection of the histograms divided by the average area of the histograms. We also assessed model log likelihood. These assessments were performed after branch length optimization to maximize likelihood.

We found that, as with the predictive metrics, all models gave similar performance, the differences of which were smaller than the differences between data sets. The overlap metric was better on the 5mer model for the held-out briney data, but was better for the CNN models for the tang data. The log likelihood was slightly better for the CNN model for all held-out data sets (**Figure 3—figure Supplement 1**).

Table 2.

Performance evaluation on held-out briney data for S5F, DeepSHM, and thrifty models.

The ∗ on S5F indicates that this model was trained using synonymous mutations on a distinct data set to those considered here. The † on tang† is to signify that this is the tang data but with a different preprocessing scheme (Tang et al., 2022).

model	training data	AUROC	AUPRC	R-prec	sub. acc.
S5F	∗	0.775	0.0698	0.0290	0.514
CNN Joined Large	tang	0.787	0.0850	0.0406	0.510
CNN Indep Medium	tang	0.786	0.0848	0.0407	0.528
CNN Indep Large	tang	0.786	0.0852	0.0406	0.524
DeepSHM	tang†	0.784	0.0865	0.0421	0.537
CNN Joined Large	tang+briney	0.793	0.0923	0.0439	0.551
CNN Indep Medium	tang+briney	0.793	0.0919	0.0441	0.560
CNN Indep Large	tang+briney	0.794	0.0926	0.0450	0.562

Table 3.

Data used in this paper.

briney data is from (Briney et al., 2019) after processing done by (Spisak et al., 2020). tang data is from Vergani et al., 2017; Tang et al., 2020 and was sequenced using the methods of Vergani et al., 2017. Out-of-frame sequences from briney and tang are used. jaffe data is from Jaffe et al., 2022 sequenced using 10X, where only 4-fold synonymous sites of productive sequences are used. The "samples" column is the number of individual samples in the dataset; in these datasets, each sample is from a distinct individual. "Clonal families" is the number of clonal families in the dataset. "PCPs" is the number of parent-child pairs in the dataset. "Median mutations" is the median number of mutations per PCP in the dataset.

purpose	name	samples	clonal families	PCPs	median mutations
train/test	briney	9	3,903	52,915	2
test	tang	21	3,209	9,984	7
train/test	jaffe	4	67,304	282,732	1

Figure 1.

(a) Overview of data processing and objective. Out-of-frame sequences are clustered into clonal families. Trees are built on clonal families and then ancestral sequences are reconstructed using a simple sequence model. The prediction task is to predict the location and identity of mutations of child sequences given parent sequences. (b) Strategy for "thrifty" CNNs with relatively few parameters. We use a trainable embedding of each 3-mer into a space; downstream convolutions happen on sequential collections of these embeddings. The "width" of the k-mer model is determined by the size of the convolutional kernel, which in this cartoon is 3. This would give us effectively a 5-mer model because the 3-mer model adds one base on either side of a convolution of length 3. For the sake of simplicity, the probability distribution of the new base conditioned on there being a substitution (which we call the conditional substitution probability or CSP) is not shown. The CSP output can emerge in several ways (**Figure 1—figure Supplement 1**).

Figure 1—figure supplement 1. Strategies for estimating both per-site rate and CSPs.

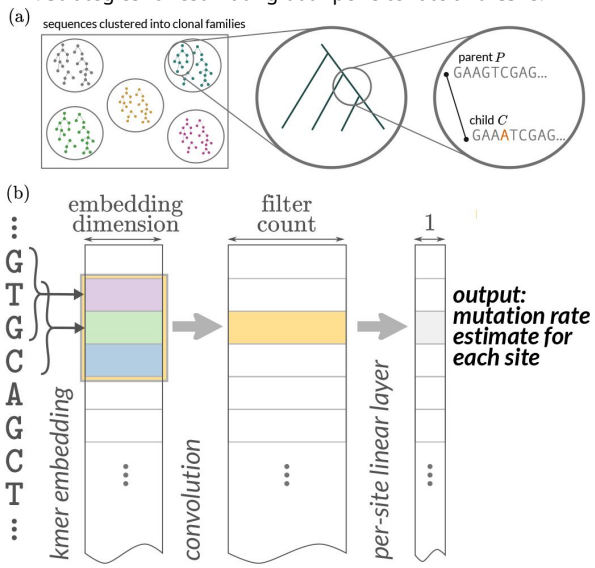

Figure 2.

Model predictive performance on held-out samples: held-out individuals from the briney data (upper row) and on a separate sequencing experiment (tang data, lower row). Integer in parentheses indicates the number of parameters of the model. Each model has multiple points, each corresponding to an independent model training. This is a subset of the models for clarity; see **Figure 2—figure Supplement 1** for all models.

Figure 2—figure supplement 1. Performance results for all the models.

Figure 2—figure supplement 2. Agreement between the original "shmoof" model of Spisak et al., 2020 and our "reshmoof" reimplementation.

Figure 2—figure supplement 3. Performance comparison including S5F model with original coefficients.

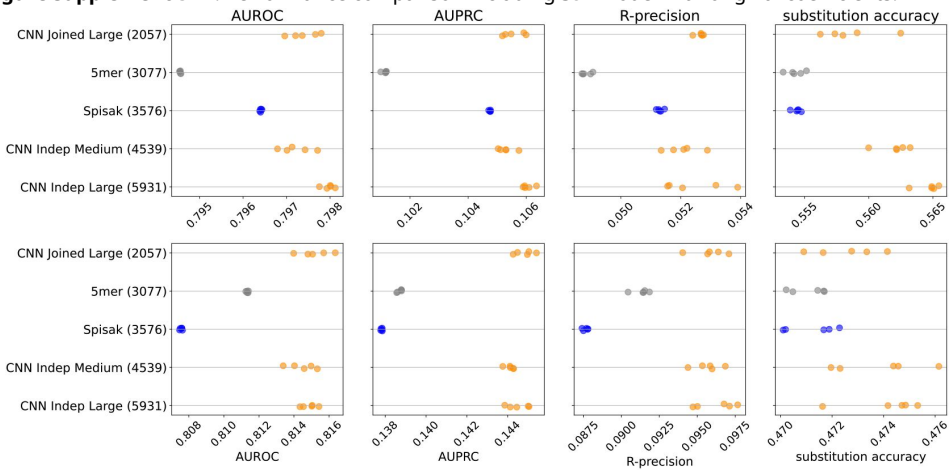

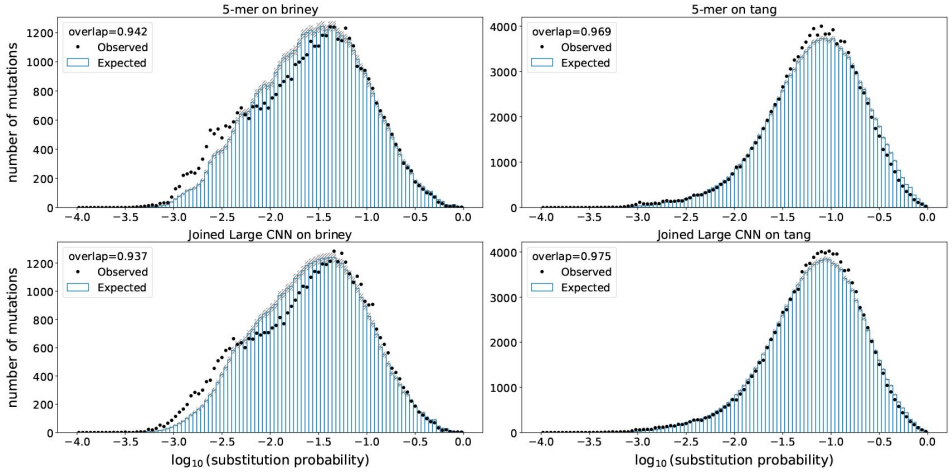

Figure 3.

Model fit on held-out samples: held-out individuals from the briney data (upper row) and on a separate sequencing experiment (tang data, lower row). Observed mutations in held-out data are placed in bins according to their probability of mutation. For every bin, the points show the observed number of mutations in that bin, while the bars show the expected number of mutations in that bin. The overlap metric is the area of the intersection of the observed and expected divided by the average area between the two.

Figure 3—figure supplement 1.

Comparison of held-out log likelihoods between the models.

Further model elaborations did not improve out of sample performance

We tried adding a per-site rate to our CNN models, as well as other elaborations such as a transformer model directly on the amino acid embeddings, and a transformer combined with a CNN. We also tried adding a positional encoding to the input for the CNN model, which does not require additional parameters, but rather perturbs the input embeddings in a way that indicates their position in the sequence (Vaswani et al., 2017). None of these elaborations improved performance on held-out data. All of these experiments can be found in notebooks in the GitHub repository associated with this paper.

We also found that jointly optimizing branch lengths along with model parameters did not improve out-of-sample performance.

Out of frame evolution and synonymous mutations give different results

We conclude from the above that the richness of these models is limited by data volume, but unfortunately we were not able to find additional data sets with many out-of-frame sequences (see end of *Methods*). This raised the question of if we can use synonymous mutations of productive sequences to augment our data set. To do so, we trained models using a combination of the original training using the briney data but also with the jaffe (Jaffe et al., 2022) data where the loss function was restricted to 4-fold synonymous sites.

We found that adding these synonymous mutations to the training set reduced performance on the held-out out-of-frame data (**Figure 4**). Furthermore, when we train in the usual way using the briney data and evaluate on our synonymous jaffe data, we do significantly worse than the S5F model, which was trained on synonymous mutations (**Figure 4—figure Supplement 1**). Our conclusion is that these two sources of data capture the effect of different processes.

Discussion

Models of somatic hypermutation are important to understand affinity maturation of B cells. They can also provide insight into the mechanism of SHM itself. Here we have developed a collection of models and worked to learn what they can teach us about SHM.

Specifically, by using an overlapping 3-mer embedding approach, we can parameterize wide-context models with relatively few parameters. For example, we can parameterize a 13-mer model with fewer parameters than a 5-mer model with better out-of-sample performance. A similar approach of embedded k-mers has been successful previously for genome regulatory element function prediction (Ji et al., 2021).

Our first main result is that these models are better than previous models using a 5-mer context, but only slightly so. This is interesting given that more distant effects are well motivated biologically, both in terms of the consensus model of somatic hypermutation involving DNA damage, stripping, and repair (Pilzecker and Jacobs, 2019), as well as more recent results showing that the mesoscale environment of the BCR is important for SHM (Wang et al., 2023). Although another model formulation may be able to pick up these features, the present approach should be able to pick up features such as a nearby AID hotspot.

We found that adding a per-site rate to our models did not help predict on out-of-sample data. This is in contrast to recent work of Spisak et al., 2020 suggesting that a per-site rate was helpful to predict SHM. We suspect that this contrast may be because of the means of evaluating this model. The Spisak et al., 2020 paper quantifies an improved model fit over a 5mer model by calculating a Pearson r^2 for each region comparing the model prediction to the aggregated mutation count per site for sites in that region. The Spisak et al., 2020 model is itself parameterized in a per-site way, and so it is not surprising that the model has excellent fit according to this metric (**Figure 4J** of Spisak et al., 2020). Although they did a data-splitting exercise, this data split was on the level of parent-child pairs (not specified in the original paper; clarified via personal communication), which means that many of the parent sequences in the training set were very similar to parent sequences in the test set. Furthermore, the baseline comparison provided in **Figure 4J** of Spisak et al., 2020 is actually not to a separately trained 5mer model, but to the 5mer component γ_w of the joint model (typo in the original paper; clarified via personal communication).

We tried other means of adding per-site rates to the model, such as positional encoding and a transformer component, but these did not help. Although it is quite possible that sites evolve differently according to their absolute position in the sequence, our work shows that this is not necessary as part of a predictive model. Due to commonalities between neighborhoods of sites in sequences, it is difficult or perhaps impossible to disentangle the effect of a per-site rate from the effect of the motif model given a sufficiently rich motif model.

Our work also contrasts the two main ways of training a neutral model: one is to use synonymous mutations (Yaari et al., 2012), and the other is to use out-of-frame sequences (Spisak et al., 2020) or some other sequences that one can assume are evolving neutrally (Cui et al., 2016). Here we find evidence that these two methods give different results, and that models trained on one task do not do well on the other. This may be from synonymous mutations being under selection due to codon usage effects, or could be from only a subset of motifs being possible to estimate from synonymous data (Yaari et al., 2013). Another possible explanation is that the spatial correlation of mutations (Spisak et al., 2020) leads to correlation in mutations at synonymous and non-synonymous sites: as an extreme example, a four-fold synonymous site could be next to a site under strong purifying selection, and if these two sites only mutate together this would effectively lead to purifying selection on the synonymous site. One could also imagine that the out-of-frame sequences are under selection such as having an insertion-deletion mutation that throws a sequence under selection out of frame, but this is mitigated by the ancestral sequence reconstruction and the removal of the naive sequence from the tree. From a model-fitting perspective, the contrast between these two objectives is disappointing, because productive sequences are much more available than out-of-frame sequences.

Overall, we have presented and tested a variety of new models with test-train splits, and found a slight improvement using parameter sparse or “thrifty” CNNs. One interesting aspect of these models is that they allow for a wider k-mer context without having a parameter explosion. It is possible that the conclusions would differ if we had considerably more data, though despite our best efforts (see Materials and Methods) we were unable to find a large additional volume of out-of-frame data. If and when additional data becomes available, our reproducible analysis can be used to evaluate these models on that data.

Materials and Methods

Data sets and data processing

Our primary dataset is the one introduced by Spisak et al. (Spisak et al., 2020) in their recent work on modeling somatic hypermutation (SHM). The data consists of human, out-of-frame IgH sequences sampled from several individuals (Briney et al., 2019), aligned using pRESTO (Vander

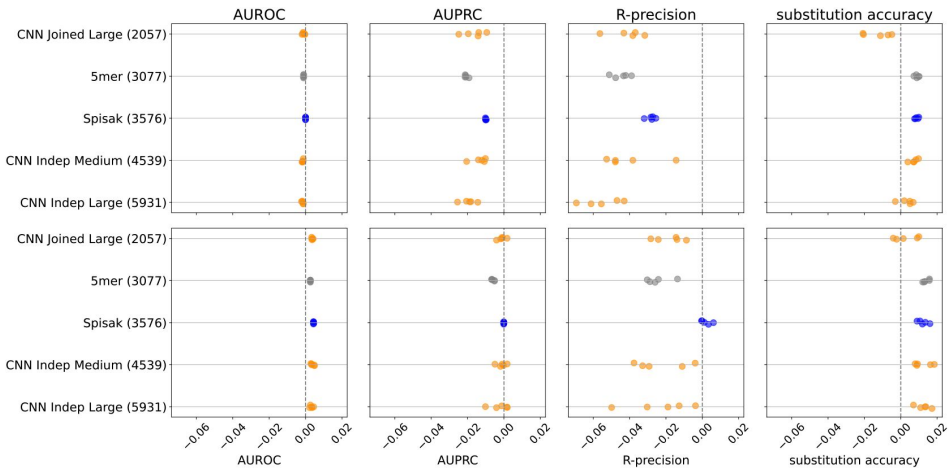

Figure 4.

The relative change in performance for each statistic, namely the statistic for the model trained with out of frame (OOF) data and synonymous data, minus the statistic for the model trained with OOF data only, divided by the statistic trained with OOF data only. Thus, adding in synonymous mutations to the training set does not help predict on held-out out-of-frame data.
Figure 4—figure supplement 1. S5F performs better for mutation position prediction on synonymous mutations in the jaffe data than any model trained on out of frame data.

Heiden et al., 2014). The resulting data comes to us as a collection of trees, one for each clonal family with at least six observed sequences in an individual, complete with (ancestral and observed) sequences and branch lengths, as well as a collection of metadata annotating, among other things, the identity and position of the V gene in the sequence. Starting from the clonal family clustering and multiple sequence alignments from (Spisak et al., 2020), we remove sequences containing gaps to avoid ambiguity of site positions due to insertions or deletions. Resulting clonal families with less than six observed sequences are discarded. Phylogenetic inference in each clonal family is then redone with IQ-TREE (Minh et al., 2020). We apply the K80 (Kimura, 1980) substitution model and use the germline sequence as an outgroup, following the method of (Spisak et al., 2020), and additionally allow for mutation rate heterogeneity among sites with a 4-category FreeR-ate model (Yang, 1995; Soubrier et al., 2012). The edges of the inferred phylogenetic trees are taken as parent-child pairs, except for the edge containing the na ive sequence outgroup.

Additionally, we use the tang data set of human IgH sequences previously used for modeling SHM by (Tang et al., 2022). This data set, originally generated by (Tang et al., 2020; Vergani et al., 2017), includes full-length BCR repertoires from 21 individuals. We obtained pre-processed samples directly from the authors (see Tang et al., 2020, for data preprocessing details). We extracted the IgH sequences from marginal zone (MZ), memory (M), and plasma (PC) B cells and completed germline and clonal family inference with partis (Ralph and Matsen, 2016a; Ralph and Matsen, 2016b; Ralph and Matsen, 2019). We keep clonal families of two or more sequences that consist of only out-of-frame sequences. In partis, a sequence is considered out-of-frame if either of the conserved codons for cysteine or tryptophan bounding the CDR3 is out-of-frame with the germline V gene. We then perform phylogenetic inference and ancestral sequence reconstruction for each clonal family using IQ-TREE as described above. The first site of the sequence is set to align with the start of the germline V gene; if necessary, nucleotides before the start of the V gene are truncated or sites at the 5' end with missing reads are padded with 'N'.

A small number of the edges have very long branch lengths, some of which seem to correspond to improper alignments. Following the lead of the authors of (Spisak et al., 2020), we filter our data to only include edges with fewer than 10 mutations, which results a modest $\sim 6.4\%$ reduction in the available data.

The jaffe data set (Jaffe et al., 2022) consists of paired heavy chain and light chain, full-length sequences of productive antibodies from four donors. We process the data with partis and IQ-TREE, similar to the tang data set. The jaffe synonymous data set are parent-child pairs from jaffe where we mask sites in the child sequence that are not 4-fold degenerate in the parent context. For each parent-child pair, we check each codon context in the parent sequence for 4-fold degenerate sites. For these sites, the corresponding nucleotide in the child sequence is preserved while all other sites are masked.

Models

In all the models we propose, we model SHM using a two-part model. First we assume that the occurrence of point mutations follows a per-site exponential waiting time that is dependent entirely on the parent sequence. Furthermore, we assume that all mutations occur simultaneously, so that we can ignore how the order of point mutations along a branch affects likelihood computations. The other output of the model is the prediction of base identity. We interpret the normalized version of these rates as conditional probabilities given that the mutation has occurred.

For the "thrifty" models, we have an embedding of each 3-mer along the sequence which is then the input for a convolutional layer (**Figure 1b**). The output of the convolutional layer is then the input for the mutation rate estimate (shown in (**Figure 1b**) as well as the CSP (**Figure 1—figure Supplement 1**).

All models are implemented in PyTorch (Paszke et al., 2019) and can be found in the GitHub repository associated with this paper.

Model training

Our loss functions are the likelihood of child mutation locations using offset, as well as a categorical cross-entropy loss for the base identity. We sum these log losses together using a weight of 0.01 on the cross-entropy loss to approximately even out the contributions of these two sources of loss.

Models were trained for 100 epochs, with the Poisson offset simply being the normalized count of mutations in the child sequence. We also tried a more sophisticated approach of joint optimization of branch length and model parameters.

Model evaluation

AUROC

The Receiver Operating Characteristic (ROC) curve is a method of visualizing the trade-off between true positive rate $(\text{TPR}=\frac{\text{TP}}{\text{TP}+\text{FN}})$ and false positive rate $(\text{FPR}=\frac{\text{FP}}{\text{TN}+\text{FP}})$ as we vary the cutoff value we use for separating positive and negative predictions. Notice that the denominators in each statistic depend only on the true labels, so the trade-off parallels the one between true positives and false positives. Given a random classifier, the TPR is expected to be equal to FPR, meaning that the ROC would be a diagonal line from (0, 0) to (1, 1).

In order to reduce the ROC curve to a single quantity for performance assessment, one can compute the area under the ROC curve (AUROC) which, when compared to 0.5, gives a sense of how well the classifier is doing when compared with a random classifier. Hanley and McNeil, 1982 show that AUROC is equivalent to probability that the classifier correctly ranks a randomly-chosen pair of points, one from the negative and one from the positive class.

AUPRC

Class imbalance, where we have many more negative examples than positive examples, can muddle performance evaluation of a classifier. Specifically, a large number of correctly-identified negative examples can obscure the relatively-poor performance of a classifier on a class that is underrepresented in the data. Another approach is to instead consider precision and recall (Saito and Rehmsmeier, 2015). Analogous to the ROC curve, the principle here is to track the precision $(\frac{\text{TP}}{\text{TP}+\text{FP}})$ and recall $(\frac{\text{TP}}{\text{TP}+\text{FN}})$ as we vary the cutoff parameter and plot the resulting points. Similar to before, we can distill the information of this curve down to a single number in the unit interval by computing the area under the precision-recall curve (AUPRC). The precision of a classifier that uniformly assigns sites to the positive and negative classes will be

$$\rho = \frac{\#\text{ mutated sites}}{\#\text{ sites}}$$

in expectation. Thus, if we exclude pathologically bad classifiers, ρ forms a base-line minimum value of the AUPRC. In contrast with the AUROC, neither precision nor recall are affected by the addition or removal of true negative (i.e. non-mutated sites that were predicted not to mutate) examples, and in fact the relationship is driven by the tradeoff between false positives and false negatives.

R-precision

In order to characterize the ability of our classifiers to correctly identify sites that will mutate we consider another metric: R-precision. This is easiest to explain by first introducing top-*k* precision, in which we take the *k* "hottest" (that is, predicted to mutate with the highest probability) sites according to our classifier and compute the precision on those sites. Therefore, in either case, we can refine top-*k* precision above to *R*-precision, which is the top-*k* precision when *k* is set equal to the expected or observed number of mutations. This value can be interpreted in the following way: an *R*-precision of 0.1 means that if the classifier is told to predict the correct sites to mutate given their count, 10% of them will have actually mutated. As with AUPRC, a random classifier will have an *R*-precision of ρ.

Substitution accuracy

As described above, when evaluating performance at predicting per-base substitution probabilities (given a mutation occurred), we report accuracy: how frequently is the predicted-most-likely base the one to which a site mutates?

Software

Our work is released in an open-source Python package *https://github.com/matsengrp/netam* with a simple API that makes it easy to train and evaluate models. We release trained models and their weights. Our analysis for this paper is reproducible via *https://github.com/matsengrp/netam-experiments-1*, which includes notebooks that reproduce the figures and tables in this paper. We used the following software: PyTorch (Paszke et al., 2019), pandas (McKinney, 2010), matplotlib (Hunter, 2007), seaborn (Waskom, 2021), snakemake (Mölder et al., 2021), pytest (Krekel et al., 2004), biopython (Cock et al., 2009).

Attempts to find additional full-length, out-of-frame sequences While the primary dataset used here and originally by Spisak et al., 2020, provides a large number of out-of-frame human IgH sequences, the sequencing methods used resulted in minimimal coverage at the start of the V gene and thus limited information for that region (Briney et al., 2019). Alternatively, the Tang dataset provides relatively high coverage along the full IgH sequence, but is limited in the amount of unique sequences sampled. We sought to supplement this data with additional full-length, out-of-frame human IgH sequences. Full-length IgH data is generally limited by design in common sequencing approaches. Even productive IgH data show low coverage at the start of the V gene, as evidenced by over 40% of the sequences in the Observed Antibody Space (OAS) database lacking sequence data for the first 15 amino acids (Olsen et al., 2022b; Kovaltsuk et al., 2018; Olsen et al., 2022a). We focus our efforts on datasets from recent studies focused on full-length antibody sequencing (Ford et al., 2023; Rodriguez et al., 2023). For all datasets, we implemented the partis-IQ-TREE pipeline as previously described on pre-processed data and extracted parent-child pairs for all clonal families of size 2+. Overall, out-of-frame sequences make up a relatively small proportion of sequence data (with this proportion varying by study/sequencing protocols) and none of the datasets considered had enough depth to extract a meaningful amount of out-of-frame sequence data for our purposes. The details of these efforts are described below. From (Ford et al., 2023), we obtained pre-processed data for 10 IgG FLAIRR-seq samples from the authors. Using consensus sequences from UMIs that were observed more than once (DUP-COUNT>1), we recovered 7,938 out-of-frame sequences across all samples. These sequences belonged to 226 clonal families of size 2+ and 2,633 singletons. This amounted to only 722 parent-child pairs, of which only 324 contained a mutation event. In attempts to extract more out-of-frame data, we additional ran our pipeline on the pre-processed data including consensus sequences that were only observed once (and thus included no UMI error correction). From the 10 samples, we were able to recover 52,785 out-of-frame sequences, some of which were not UMI error corrected. This resulted in 2,415 clonal families of size 2+ and 22,983 singletons, but still only gave us 6,296 parent-

child pairs with mutation events (9,114 in total). We note that this sequencing method provided a higher proportion of out-of-frame sequences (9% for fully pre-processed data) than other methods we considered.

Acknowledgements

Thank you to the authors of (Spisak et al., 2020) for providing the data and answering questions about their work. We are also grateful to the authors of (Tang et al., 2022) for providing the data and answering questions about their work, as well as to the lab of Corey Watson for sharing data. This work supported by NIH grant R01-AI146028. Scientific Computing Infrastructure at Fred

Hutch funded by ORIP grant S10OD028685. Frederick Matsen is an investigator of the Howard Hughes Medical Institute.

This work was partially completed at the Kavli Institute for Theoretical Physics (KITP) at the University of California, Santa Barbara, and thus was supported by grant no. NSF PHY-2309135 to the Kavli Institute for Theoretical Physics (KITP) and the Gordon and Betty Moore Foundation Grant No. 2919.02.

Figure 1–figure supplement 1.

Our three strategies for estimating the per-site rate and CSPs. In the joined version, the two outputs come directly out of the convolutional layer. In the hybrid version, the two outputs share the embedding layer. In the independent version, the two outputs are estimated separately.

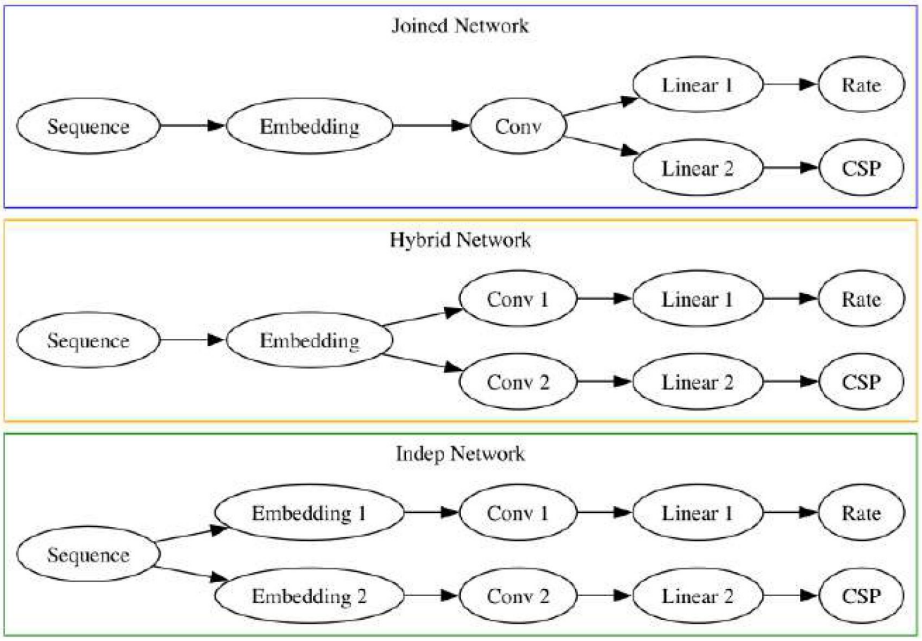

Figure 2–figure supplement 1.

Performance results for all the models.

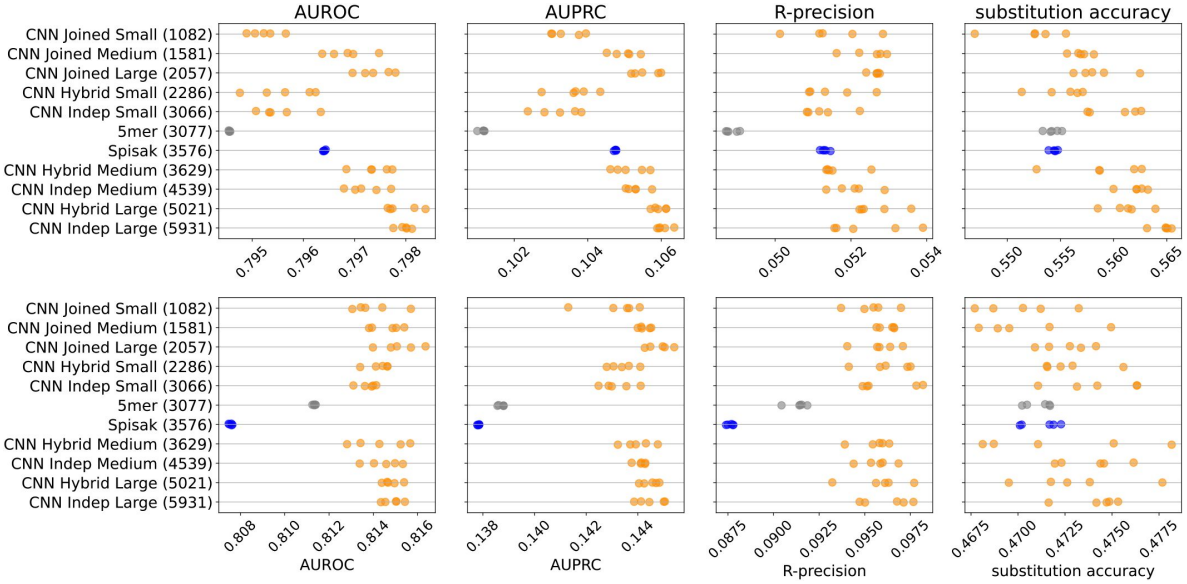

Figure 2–figure supplement 2.

There is good agreement between the originally inferred shmoof coefficients and our re-implementation, both in the motif mutability terms and the per-position mutabilities. The primary exception is that we infer more reasonable values when sequencing coverage is weak or absent and avoid an extreme value at site 67. These are due to a slight regularization to the per-position mutabilities.This analysis can be reproduced using the reshmoof.ipynb notebook.

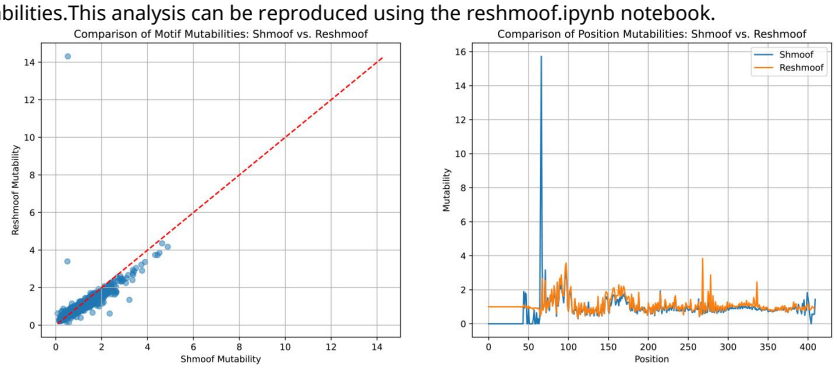

Figure 2–figure supplement 3.

Performance plot including the original S5F model (vertical black lines) for held-out individuals from the briney data (upper row) and on a separate sequencing experiment (tang data, lower row).

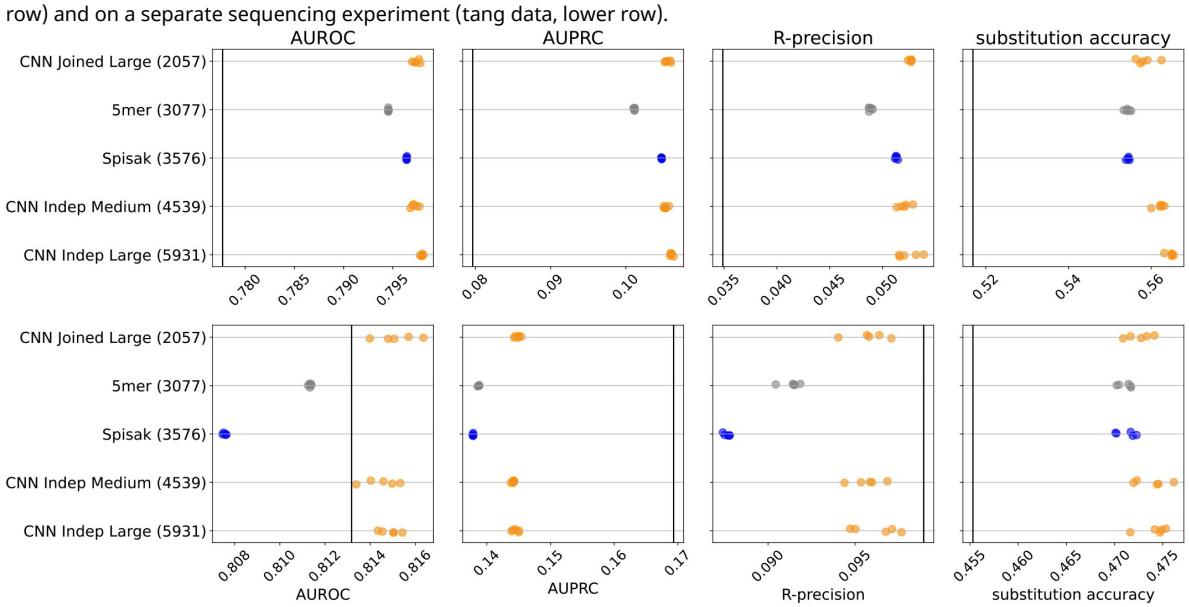

Figure 3–figure supplement 1.

Comparison of held-out log likelihoods between the models.

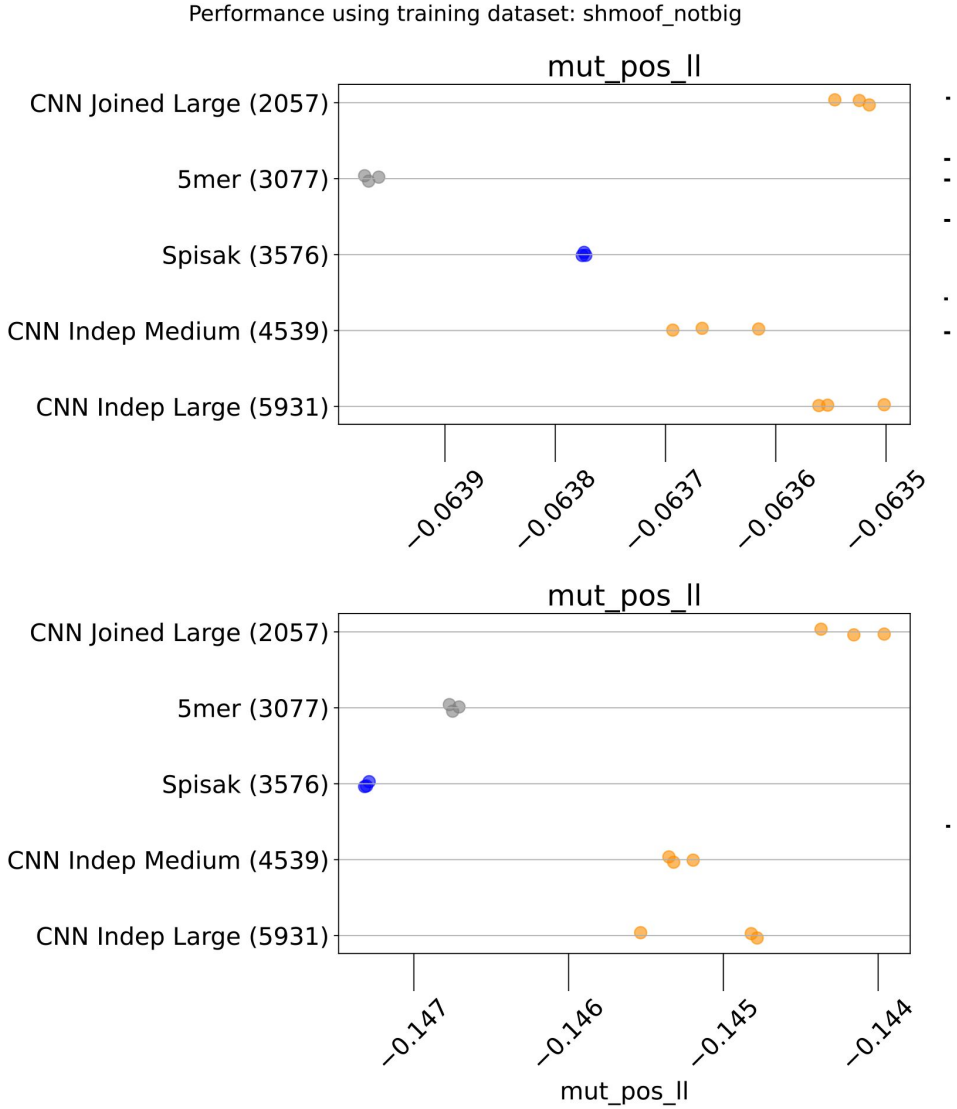

Figure 4–figure supplement 1.

S5F performs better for mutation position prediction on synonymous mutations in the jaffe data than any model trained on out of frame data. Performance plot is as before, but black vertical bar indicates the performance of the S5F model, and all models evaluated on synonymous mutations in the jaffe data.

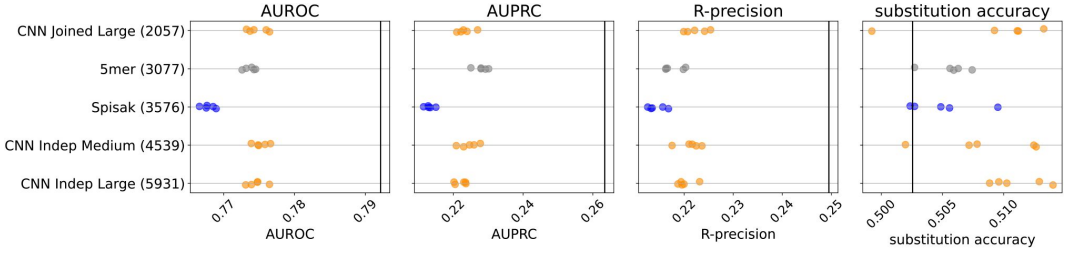

References

Briney B, Inderbitzin A, Joyce C, Burton DR 2019) **Commonality despite exceptional diversity in the baseline human antibody repertoire** *Nature* **566**:393–397

Cock PJA, Antao T, Chang JT, Chapman BA, Cox CJ, Dalke A, Friedberg I, Hamelryck T, Kauff F, Wilczynski B, de Hoon MJL. 2009) **Biopython: freely available Python tools for computational molecular biology and bioinformatics** *Bioinformatics* **25**:1422–1423 https://doi.org/10.1093/bioinformatics/btp163

Cohen RM, Kleinstein SH, Louzoun Y. 2011) **Somatic hypermutation targeting is influenced by location within the immunoglobulin V region** *Mol Immunol* **48**:1477–1483 https://doi.org/10.1016/j.molimm.2011.04.002

Cui A, Di Niro R, Vander Heiden JA, Briggs AW, Adams K, Gilbert T, O'Connor KC, Vigneault F, Shlomchik MJ, Kleinstein SH 2016) **A Model of Somatic Hypermutation Targeting in Mice Based on High-Throughput Ig Sequencing Data** *J Immunol* **197**:3566–3574 https://doi.org/10.4049/jimmunol.1502263

Dunn-Walters DK, Dogan A, Boursier L, MacDonald CM, Spencer J. 1998) **Base-specific sequences that bias somatic hypermutation deduced by analysis of out-of-frame human IgVH genes** *J Immunol* **160**:2360–2364

Elhanati Y, Sethna Z, Marcou Q, Callan CG, Mora T, Walczak AM 2015) **Inferring processes underlying B-cell repertoire diversity** *Philos Trans R Soc Lond B Biol Sci* **370** https://doi.org/10.1098/rstb.2014.0243

Feng J, Shaw DA, Minin VN, Simon N, Matsen FA IV 2019) **Survival analysis of DNA mutation motifs with penalized pro-portional hazards** *Ann Appl Stat* **13**:1268–1294 https://doi.org/10.1214/18-AOAS1233

Fisher T, Sung K, Simon N, Fukuyama J, Matsen FA 2024) **Inferring mechanistic parameters of somatic hypermutation using neural networks and approximate Bayesian computation** *Annals of Applied Statistics*

Ford EE, Tieri D, Rodriguez OL, Francoeur NJ, Soto J, Kos JT, Peres A, Gibson WS, Silver CA, Deikus G, Hudson E, Woolley CR, Beckmann N, Charney A, Mitchell TC, Yaari G, Sebra RP, Watson CT, Smith ML 2023) **FLAIRR-seq: A method for single-molecule resolution of near full-length antibody H chain repertoires** *J Immunol* **210**:1607–1619 https://doi.org/10.4049/jimmunol.2200825

Hanley JA, McNeil BJ 1982) **The meaning and use of the area under a receiver operating characteristic (ROC) curve** *Radiology* **143**:29–36

Hoehn KB, Lunter G, Pybus OG 2017) **A Phylogenetic Codon Substitution Model for Antibody Lineages** *Genetics* **206**:417–427 https://doi.org/10.1534/genetics.116.196303

Hoehn KB, Vander Heiden JA, Zhou JQ, Lunter G, Pybus OG, Kleinstein SH 2019) **Repertoire-wide phylogenetic models of B cell molecular evolution reveal evolutionary signatures of aging and vaccination** *Proc Natl Acad Sci U S A* https://doi.org/10.1073/pnas.1906020116

Hunter JD 2007) **Matplotlib: A 2D graphics environment** *Computing in Science & Engineering* **9**:90–95 https://doi.org/10.1109/MCSE.2007.55

Jaffe DB, Shahi P, Adams BA, Chrisman AM, Finnegan PM, Raman N, Royall AE, Tsai F, Vollbrecht T, Reyes DS, Hepler NL, McDonnell WJ 2022) **Functional antibodies exhibit light chain coherence** *Nature* **611**:352–357 https://doi.org/10.1038/s41586-022-05371-z

Ji Y, Zhou Z, Liu H, Davuluri RV 2021) **DNABERT: pre-trained Bidirectional Encoder Representations from Transformers model for DNA-language in genome** *Bioinformatics* **37**:2112–2120 https://doi.org/10.1093/bioinformatics/btab083

Kimura M. 1980) **A simple method for estimating evolutionary rates of base substitutions through comparative studies of nucleotide sequences** *Journal of Molecular Evolution* **16**:111–120 https://doi.org/10.1007/BF01731581

Kovaltsuk A, Leem J, Kelm S, Snowden J, Deane CM, Krawczyk K. 2018) **Observed Antibody Space: A resource for data mining next-generation sequencing of antibody repertoires** *J Immunol* **201**:2502–2509 https://doi.org/10.4049/jimmunol.1800708

Krekel H, Oliveira B, Pfannschmidt R, Bruynooghe F, Laugher B, Bruhin F 2004) **pytest** *GitHub* https://github.com/pytest-dev/pytest

Levinstein Hallak K, Rosset S. 2022) **Statistical modeling of SARS-CoV-2 substitution processes: predicting the next variant** *Commun Biol* **5**:285 https://doi.org/10.1038/s42003-022-03198-y

Levinstein Hallak K, Tzur S, Rosset S. 2018) **Big data analysis of human mitochondrial DNA substitution models: a regression approach** *BMC Genomics* **19**:759 https://doi.org/10.1186/s12864-018-5123-x

Marcou Q, Mora T, Walczak AM 2018) **High-throughput immune repertoire analysis with IGoR** *Nat Commun* **9**:561 https://doi.org/10.1038/s41467-018-02832-w

Martin Beem JS, Venkatayogi S, Haynes BF, Wiehe K. 2023) **ARMADiLLO: a web server for analyzing antibody mutation probabilities** *Nucleic Acids Res* **51**:W51–W56 https://doi.org/10.1093/nar/gkad398

McCoy CO, Bedford T, Minin VN, Bradley P, Robins H, Matsen FA IV 2015) **Quantifying evolutionary constraints on B-cell affinity maturation** *Philos Trans R Soc Lond B Biol Sci* **370** https://doi.org/10.1098/rstb.2014.0244

McKinney W 2010) **Data Structures for Statistical Computing in Python** In: *Proceedings of the 9th Python in Science Conference* pp. 56–61 https://doi.org/10.25080/Majora-92bf1922-00a

Methot SP, Di Noia JM, Alt Frederick W 2017) **Chapter Two - Molecular Mechanisms of Somatic Hypermutation and Class Switch Recombination** In: *Advances in Immunology* Academic Press pp. 37–87 https://doi.org/10.1016/bs.ai.2016.11.002

Minh BQ, Schmidt HA, Chernomor O, Schrempf D, Woodhams MD, von Haeseler A, Lanfear R. 2020) **IQ-TREE 2: New Models and Efficient Methods for Phylogenetic Inference in the Genomic Era** *Molecular Biology and Evolution* **37**:1530–1534 https://doi.org/10.1093/molbev/msaa015

Mölder F, Jablonski K, Letcher B, Hall M, Tomkins-Tinch C, Sochat V, Forster J, Lee S, Twardziok S, Kanitz A, Wilm A, Holtgrewe M, Rahmann S, Nahnsen S, Köster J. 2021) **Sustainable data analysis with Snakemake [version 2; peer review: 2 approved]** *F1000Research* **10** https://doi.org/10.12688/f1000research.29032.2

Olsen TH, Boyles F, Deane CM 2022) **Observed Antibody Space: A diverse database of cleaned, annotated, and translated unpaired and paired antibody sequences** *Protein Sci* **31**:141–146 https://doi.org/10.1002/pro.4205

Olsen TH, Moal IH, Deane CM 2022) **AbLang: an antibody language model for completing antibody sequences** *Bioinform Adv* **2**:vbac046 https://doi.org/10.1093/bioadv/vbac046

Ozenne B, Subtil F, Maucort-Boulch D. 2015) **The precision–recall curve overcame the optimism of the receiver operating characteristic curve in rare diseases** *J Clin Epidemiol* **68**:855–859 https://doi.org/10.1016/j.jclinepi.2015.02.010

Paszke A, Gross S, Massa F, Lerer A, Bradbury J, Chanan G, Killeen T, Lin Z, Gimelshein N, Antiga L, Desmaison A, Köpf A, Yang E, DeVito Z, Raison M, Tejani A, Chilamkurthy S, Steiner B, Fang L, Bai J, et al. 2019) **PyTorch: An imperative style, high-performance deep learning library** *arXiv* https://doi.org/10.48550/arXiv.1912.01703

Pilzecker B, Jacobs H. 2019) **Mutating for Good: DNA Damage Responses During Somatic Hypermutation** *Front Immunol* **10**:438 https://doi.org/10.3389/fimmu.2019.00438

Ralph DK, Matsen FA IV 2016) **Consistency of VDJ rearrangement and substitution parameters enables accurate B cell receptor sequence annotation** *PLoS Comput Biol* **12**:e1004409 https://doi.org/10.1371/journal.pcbi.1004409

Ralph DK, Matsen FA IV 2016) **Likelihood-based inference of B cell clonal families** *PLoS Comput Biol* **12**:e1005086 https://doi.org/10.1371/journal.pcbi.1005086

Ralph DK, Matsen FA IV 2019) **Per-sample immunoglobulin germline inference from B cell receptor deep sequencing data** *PLoS Comput Biol* **15**:e1007133 https://doi.org/10.1371/journal.pcbi.1007133

Rodriguez OL, Safonova Y, Silver CA, Shields K, Gibson WS, Kos JT, Tieri D, Ke H, Jackson KJL, Boyd SD, Smith ML, Marasco WA, Watson CT 2023) **Genetic variation in the immunoglobulin heavy chain locus shapes the human antibody repertoire** *Nature Comm* **14**:4419 https://doi.org/10.1038/s41467-023-40070-x

Rogozin IB, Kolchanov NA 1992) **Somatic hypermutagenesis in immunoglobulin genes. II. Influence of neighbouring base sequences on mutagenesis** *Biochim Biophys Acta* **1171**:11–18 https://doi.org/10.1016/0167-4781(92)90134-l

Rogozin IB, Diaz M. 2004) **Cutting edge: DGYW/WRCH is a better predictor of mutability at G:C bases in Ig hypermutation than the widely accepted RGYW/WRCY motif and probably reflects a two-step activation-induced cytidine deaminase-triggered process** *J Immunol* **172**:3382–3384 https://doi.org/10.4049/jimmunol.172.6.3382

Rosset S. 2007) **Efficient inference on known phylogenetic trees using Poisson regression** *Bioinformatics* **23**:e142–7 https://doi.org/10.1093/bioinformatics/btl306

Saito T, Rehmsmeier M. 2015) **The Precision-Recall Plot Is More Informative than the ROC Plot When Evaluating Binary Classifiers on Imbalanced Datasets** *PLOS One*

10:e0118432 https://doi.org/10.1371/journal.pone.0118432

Soubrier J, Steel M, Lee MSY, Der Sarkissian C, Guindon S, Ho SYW, Cooper A. 2012) **The Influence of Rate Heterogeneity among Sites on the Time Dependence of Molecular Rates** *Molecular Biology and Evolution* **29**:3345–3358 https://doi.org/10.1093/molbev/mss140

Spisak N, Walczak AM, Mora T. 2020) **Learning the heterogeneous hypermutation landscape of immunoglobulins from high-throughput repertoire data** *Nucleic Acids Res* **48**:10702–10712 https://doi.org/10.1093/nar/gkaa825

Tang C, Bagnara D, Chiorazzi N, Scharff MD, MacCarthy T. 2020) **AID overlapping and Polη hotspots are key features of evolutionary variation within the human antibody heavy chain (IGHV) genes** *Front Immunol* **11**:788 https://doi.org/10.3389/fimmu.2020.00788

Tang C, Krantsevich A, MacCarthy T. 2022) **Deep learning model of somatic hypermutation reveals importance of sequence context beyond hotspot targeting** *iScience* **25**:103668 https://doi.org/10.1016/j.isci.2021.103668

Teng G, Papavasiliou FN 2007) **Immunoglobulin somatic hypermutation** *Annu Rev Genet* **41**:107–120 https://doi.org/10.1146/annurev.genet.41.110306.130340

Vander Heiden JA, Yaari G, Uduman M, Stern JNH, O'Connor KC, Hafler DA, Vigneault F, Kleinstein SH 2014) **pRESTO: a toolkit for processing high-throughput sequencing raw reads of lymphocyte receptor repertoires** *Bioinformatics* **30**:1930–1932 https://doi.org/10.1093/bioinformatics/btu138

Vaswani A, Shazeer N, Parmar N, Uszkoreit J, Jones L, Gomez AN, Lu Kaiser, Polosukhin I. 2017) **Attention is All you Need** In: *31st Conference on Neural Information Processing Systems*

Vergani S, Korsunsky I, Mazzarello AN, Ferrer G, Chiorazzi N, Bagnara D. 2017) **Novel method for high-throughput full-length IGHV-D-J sequencing of the immune repertoire from bulk B-cells with single-cell resolution** *Front Immunol* **8**:1157 https://doi.org/10.3389/fimmu.2017.01157

Wagner SD, Neuberger MS 1996) **Somatic hypermutation of immunoglobulin genes** *Annu Rev Immunol* **14**:441–457 https://doi.org/10.1146/annurev.immunol.14.1.441

Wang Y, Zhang S, Yang X, Hwang JK, Zhan C, Lian C, Wang C, Gui T, Wang B, Xie X, Dai P, Zhang L, Tian Y, Zhang H, Han C, Cai Y, Hao Q, Ye X, Liu X, Liu J, et al. 2023) **Mesoscale DNA feature in antibody-coding sequence facilitates somatic hypermutation** *Cell* https://doi.org/10.1016/j.cell.2023.03.030

Waskom ML 2021) **seaborn: statistical data visualization** *Journal of Open Source Software* **6**:3021 https://doi.org/10.21105/joss.03021

Wiehe K, Bradley T, Ryan Meyerhoff R, Hart C, Williams WB, Easterhoff D, Faison WJ, Kepler TB, Saunders KO, Munir Alam S, Bonsignori M, Haynes BF 2018) **Functional Relevance of Improbable Antibody Mutations for HIV Broadly Neutralizing Antibody Development** *Cell Host Microbe* **0** https://doi.org/10.1016/j.chom.2018.04.018

Wiehe K, Saunders KO, Stalls V, Cain DW, Venkatayogi S, Martin Beem JS, Berry M, Evangelous T, Henderson R, Hora B, Xia SM, Jiang C, Newman A, Bowman C, Lu X, Bryan ME, Bal J, Sanzone A, Chen H, Eaton A, et al. 2022) **Mutation-Guided Vaccine Design: A Strategy for Developing**

Boosting Immunogens for HIV Broadly Neutralizing Antibody Induction *bioRxiv* https://doi.org/10.1101/2022.11.11.516143

Yaari G, Uduman M, Kleinstein SH 2012) **Quantifying selection in high-throughput Immunoglobulin sequencing data sets** *Nucleic Acids Res* **40**:e134 https://doi.org/10.1093/nar/gks457

Yaari G, Vander Heiden JA, Uduman M, Gadala-Maria D, Gupta N, Stern JNH, O'Connor KC, Hafler DA, Laserson U, Vigneault F, Kleinstein SH 2013) **Models of somatic hypermutation targeting and substitution based on synonymous mutations from high-throughput immunoglobulin sequencing data** *Front Immunol* **4**:358 https://doi.org/10.3389/fimmu.2013.00358

Yang Z. 1995) **A space-time process model for the evolution of DNA sequences** *Genetics* **139**:993–1005 https://doi.org/10.1093/genetics/139.2.993

Zhou JQ, Kleinstein SH 2020) **Position-Dependent Differential Targeting of Somatic Hypermutation** *J Immunol* https://doi.org/10.4049/jimmunol.2000496

Author information

Kevin Sung
Computational Biology Program, Fred Hutchinson Cancer Center, Seattle, United States
ORCID iD: 0000-0002-7289-845X

Mackenzie M Johnson
Computational Biology Program, Fred Hutchinson Cancer Center, Seattle, United States
ORCID iD: 0000-0002-3915-2023

Will Dumm
Computational Biology Program, Fred Hutchinson Cancer Center, Seattle, United States
ORCID iD: 0000-0002-8617-476X

Noah Simon
Department of Biostatistics, University of Washington, Seattle, United States
ORCID iD: 0000-0002-8985-2474

Hugh Haddox
Computational Biology Program, Fred Hutchinson Cancer Center, Seattle, United States
ORCID iD: 0000-0001-8324-8324

Julia Fukuyama
Department of Statistics, Indiana University, Bloomington, United States
ORCID iD: 0000-0002-7590-5563

Frederick A Matsen IV
Howard Hughes Medical Institute, Seattle, United States, Department of Genome Sciences, University of Washington, Seattle, United States, Department of Statistics, University of Washington, Seattle, United States
ORCID iD: 0000-0003-0607-6025

For correspondence: matsen@fredhutch.org

Editors

Reviewer #1 (Public review):

Summary:

This paper introduces a new class of machine learning models for capturing how likely a specific nucleotide in a rearranged IG gene is to undergo somatic hypermutation. These models modestly outperform existing state-of-the-art efforts, despite having fewer free parameters. A surprising finding is that models trained on all mutations from non-functional rearrangements give divergent results from those trained on only silent mutations from functional rearrangements.

Strengths:

(1) The new model structure is quite clever and will provide a powerful way to explore larger models.

(2) Careful attention is paid to curating and processing large existing data sets.

(3) The authors are to be commended for their efforts to communicate with the developers of previous models and use the strongest possible versions of those in their current evaluation.

Weaknesses:

(1) 10x/single cell data has a fairly different error profile compared to bulk data. A synonymous model should be built from the same ḃriney ̀dataset as the base model to validate the difference between the two types of training data.

(3) The decision to test only kernels of 7, 9, and 11 is not described. The selection/optimization of embedding size is not explained. The filters listed in Table 1 are not defined.

https://doi.org/10.7554/eLife.105471.1.sa2

Reviewer #2 (Public review):

This work offers an insightful contribution for researchers in computational biology, immunology, and machine learning. By employing a 3-mer embedding and CNN architecture, the authors demonstrate that it is possible to extend sequence context without exponentially increasing the model's complexity.

Key findings include:

(1) Efficiency and Performance: Thrifty CNNs outperform traditional 5-mer models and match the performance of significantly larger models like DeepSHM.

(2) Neutral Mutation Data: A distinction is made between using synonymous mutations and out-of-frame sequences for model training, with evidence suggesting these methods capture different aspects of SHM, or different biases in the type of data.

(3) Open Source Contributions: The release of a Python package and pre-trained models adds practical value for the community.

However, readers should be aware of the limitations. The improvements over existing models are modest, and the work is constrained by the availability of high-quality out-of-frame sequence data. The study also highlights that more complex modeling techniques, like transformers, did not enhance predictive performance, which underscores the role of data availability in such studies.

https://doi.org/10.7554/eLife.105471.1.sa1

Reviewer #3 (Public review):

Summary:

Modeling and estimating sequence context biases during B cell somatic hypermutation is important for accurately modeling B cell evolution to better understand responses to infection and vaccination. Sung et al. introduce new statistical models that capture a wider sequence context of somatic hypermutation with a comparatively small number of additional parameters. They demonstrate their model's performance with rigorous testing across multiple subjects and datasets. Prior work has captured the mutation biases of fixed 3-, 5-, and 7-mers, but each of these expansions has significantly more parameters. The authors developed a machine-learning-based approach to learn these biases using wider contexts with comparatively few parameters.

Strengths:

Well-motivated and defined problem. Clever solution to expand nucleotide context. Complete separation of training and test data by using different subjects for training vs testing. Release of open-source tools and scripts for reproducibility.

Weaknesses:

This study could be improved with better descriptions of dataset sequencing technology, sequencing depth, etc but this is a minor weakness.

https://doi.org/10.7554/eLife.105471.1.sa0